tvst

Article

Noninvasive Imaging of Cone Ablation and Regeneration in Zebrafish

Alison L. Huckenpahler[1], Nicole A. Lookfong[2], Emma Warr[3], Elizabeth Heffernan[3], Joseph Carroll[1,3], and Ross F. Collery[1,3]

[1] Cell Biology, Neurobiology & Anatomy, Medical College of Wisconsin, Milwaukee, WI, USA
[2] Penn State Harrisburg, Harrisburg, PA, USA
[3] Ophthalmology & Visual Sciences, Medical College of Wisconsin, Milwaukee, WI, USA

Correspondence: Ross F. Collery, Department of Ophthalmology & Visual Sciences, Medical College of Wisconsin Eye Institute, 925 N 87th St, Milwaukee, WI 53226-0509, USA. e-mail: rcollery@mcw.edu

Received: April 1, 2020
Accepted: August 12, 2020
Published: September 16, 2020

Keywords: zebrafish; OCT; regeneration; Müller cell; cone photoreceptor

Citation: Huckenpahler AL, Lookfong NA, Warr E, Heffernan E, Carroll J, Collery RF. Noninvasive imaging of cone ablation and regeneration in zebrafish. Trans Vis Sci Tech. 2020;9(10):18, https://doi.org/10.1167/tvst.9.10.18

Purpose: To observe and characterize cone degeneration and regeneration in a selective metronidazole-mediated ablation model of ultraviolet-sensitive (UV) cones in zebrafish using in vivo optical coherence tomography (OCT) imaging.

Methods: Twenty-six *sws1:nfsB-mCherry;sws2:eGFP* zebrafish were imaged with OCT, treated with metronidazole to selectively kill UV cones, and imaged at 1, 3, 7, 14, 28, or 56 days after ablation. Regions 200 × 200 µm were cropped from volume OCT scans to count individual UV cones before and after ablation. Fish eyes were fixed, and immunofluorescence staining was used to corroborate cone density measured from OCT and to track monocyte response.

Results: Histology shows significant loss of UV cones after metronidazole treatment with a slight increase in observable blue cone density one day after treatment (Kruskal, Wallis, $P = 0.0061$) and no significant change in blue cones at all other timepoints. Regenerated UV cones measured from OCT show significantly lower density than pre-cone-ablation at 14, 28, and 56 days after ablation (analysis of variance, $P < 0.01$, $P < 0.0001$, $P < 0.0001$, respectively, 15.9% of expected nonablated levels). Histology shows significant changes to monocyte morphology (mixed-effects analysis, $P < 0.0001$) and retinal position (mixed-effects analysis, $P < 0.0001$).

Conclusions: OCT can be used to observe loss of individual cones selectively ablated by metronidazole prodrug activation and to quantify UV cone loss and regeneration in zebrafish. OCT images also show transient changes to the blue cone mosaic and inner retinal layers that occur concomitantly with selective UV cone ablation.

Translational Relevance: Profiling cone degeneration and regeneration using in vivo imaging enables experiments that may lead to a better understanding of cone regeneration in vertebrates.

Introduction

Zebrafish are an important model organism. Their cone-rich retinas, low husbandry costs, and abundant genetic tools make them an attractive model for studying vision and vision disorders.[1] However, beyond these advantages, zebrafish also possess the ability to regenerate postmitotic cone photoreceptors by dedifferentiating Müller glia into multipotent stem cells.[2–4] Thus there is significant interest in studying retinal regeneration in the zebrafish,[5] because understanding the molecular cues and pathways initiated by retinal damage and subsequent regeneration of retinal neurons in zebrafish may ultimately lead to therapeutic advances in restoring lost photoreceptors in human visual disease.[6,7] Although researchers have discovered several factors and processes that drive zebrafish retinal regeneration, much remains to be understood.[4,8] However, most of the studies investigating this phenomenon rely on post-mortem histology, which prevents in vivo longitudinal study and limits

the ability to correlate changes in photoreceptors to changes in visual perception. Using noninvasive imaging techniques could enable more in-depth study of loss and regeneration of cone photoreceptors in vivo and inform researchers on structure-function studies.[9]

Optical coherence tomography (OCT) is a widely-used clinical technology for noninvasive assessment of the retina.[10] OCT has an axial resolution that allows researchers to view individual retinal layers in humans, with some systems achieving an axial resolution of less than 5 µm.[11] Although commercial systems lack cellular resolution, research-grade OCT systems equipped with adaptive optics are capable of resolving individual photoreceptors,[12] as well as ganglion cells[13] and retinal pigment epithelium[14] in the living human retina. In recent years, OCT has been applied to a number of animal models,[15–20] including zebrafish.[21–25] In zebrafish, OCT has broad applications; it has been used to measure axial length,[21] image the lens,[25] retinal nerve fiber layers,[26] and retinal melanin.[22,23] In addition, commercial OCT has been used by multiple groups to noninvasively image the zebrafish cone mosaic with single cell resolution.[26–28] Moreover, because OCT is a reflectance-based imaging modality, it does not require transgenic lines or exogenous contrast agents for imaging of photoreceptors.

Recent studies by Huckenpahler et al.[29] and Toms et al.[28] have demonstrated longitudinal imaging of the wild-type zebrafish UV cone mosaic, phylogenetically corresponding to blue cones in humans and S-cones in mice. Imaging individual cones opens up the possibility of using OCT to monitor cone degeneration in disease models. OCT has been used to study cone degeneration but had only tracked indirect measures of cone health, such as outer nuclear layer (ONL) thickness or qualitative appearance.[26,30] Several previous studies of zebrafish retinal regeneration have induced nonspecific retinal degeneration[30–34] and ablated multiple cell types or large pieces of the retina. In this work, we selectively ablate a single cone subtype using an approach that limits cell death to only those expressing a bacterial enzyme which is harmless until exposed to an exogenous prodrug metronidazole.[35–37] Metronidazole is activated through reduction and kills cells expressing the nitroreductase enzyme, leaving cells immediately surrounding it unharmed. This approach allows us to observe ultraviolet-sensitive (UV) cones after their selective ablation with OCT imaging. Here we combine noninvasive OCT imaging with cross-sectional correlative histology to characterize cone degeneration and regeneration in a selective UV-cone ablation model of zebrafish using in vivo OCT imaging.

Methods

Zebrafish Models and Experimental Design

Zebrafish studies were approved by the Institutional Animal Care and Use Committee at the Medical College of Wisconsin and conducted in accordance with the ARVO Statement for the Use of Animals in Ophthalmic and Vision Research. We used 26 adult *sws1:nfsB-mCherry;sws2:eGFP* zebrafish (ZFIN ID q30Tg for *sws1:nfsB-mCherry*; fish sent from Rachel Wong's laboratory[38]) between the ages of 12 and 36 months of age. The zebrafish were imaged before and after selective metronidazole-mediated ablation of the UV-cone mosaic. Metronidazole is a commonly used antibiotic and a prodrug, which is only converted into a cytotoxic agent by bacteria or cells expressing the cloned *Escherichia coli nsfB*–activating gene, which then kills those cells while leaving their immediate neighbors unaffected.[39] Metronidazole is commercially sourced as a powder (Millipore Sigma, Burlington, MA, USA; catalog number M3761) that is dissolved in aquarium water to a final concentration of 10 mmol/L before treatment of fish. Of the 26 fish expressing the *nsfB* gene, 18 fish were imaged before cone ablation (before ablation) and then again at a single timepoint after ablation (three fish each at 1, 3, 7, 14, 28, or 56 days). Three fish were imaged and then sacrificed before cone ablation (nonablation fish). Four fish had preablation imaging done and were kept as extras in case of death, and one fish was excluded because of observed skeletal abnormalities.

Optical Coherence Tomography Imaging

Before imaging, fish were anesthetized in 168 mg/L tricaine solution (Millipore Sigma; catalog number E10521). We used a Bioptigen Envisu R2200 SD-OCT (Bioptigen, Research Triangle Park, NC, USA) with a broadband source (central wavelength 878.4 nm, 186.3 nm bandwidth; Superlum, Enterprise Park, Cork, Ireland) to acquire line (1.2 mm, 80 B-scans, 500 A scans/B-scan) and volume scans (nominal scan size 1.2 × 1.2 mm, 500 B-scans, 500 A scans/B-scan) of the retina following the procedure in Huckenpahler et al.[27] The true lateral dimensions of the OCT scans were determined by measuring axial length as previously described in Collery et al.[21] and the lateral scaling determined with the measured axial length according to the formula in Huckenpahler et al.[27] Actual OCT scan size was 429 to 619 µm. After baseline imaging, the fish were allowed to recover

and then incubated in 10 mmol/L metronidazole for 24 hours. After the UV cone ablation by metronidazole treatment, fish were returned to the water-circulating system and allowed to recover for 1, 3, 7, 14, 28, or 56 days after ablation (DPA) before being imaged again; three fish were imaged at each timepoint and sacrificed for immunohistochemistry.

Bioptigen OCT volume scans were processed by creating a custom contour of the retina to include layers of interest as previously shown.[27] Twenty frames from B-scans were registered and averaged as previously described.[40] We cropped 200- × 200-µm regions of interest from the en face volume OCT scans. The UV cones were identified on the baseline scan using their distinct appearance and location in retinal sublamina. The distance between the UV contour and the retinal pigment epithelium (RPE) was measured and UV contour generated at the same retinal position on the postablation OCT scans. These scans were manually counted and then density and nearest neighbor distance calculated from the counts using custom software (Translational Imaging Innovations, Inc., Hickory, NC, USA).[41]

Cryohistology

Following post-ablation OCT imaging, fish were sacrificed and fixed in 4% paraformaldehyde for 24 hours. The fixed fish were then decapitated before being sucrose-treated and embedded in Tissue-Tek O.C.T. Compound (Sakura Finetek, Torrance, CA, USA) for cryoembedding and histology. Cryofixed heads were sliced in 12 µm thick sections and stained with TO-PRO-3 (Thermo Fisher Scientific, Inc., Waltham, MA, USA) or stained with either 4C4 antibody against fish leukocytes (gift from Peter Hitchcock, University of Michigan[42]) and far-red secondary antibody (goat anti-mouse 633; Invitrogen, Carlsbad, CA, USA), or GFAP antibody (mouse anti-GFAP; Abcam, Cambridge, UK) and far-red secondary antibody. Slides were imaged on a Nikon Eclipse E600FN (Nikon Corporation, Tokyo, Japan) confocal microscope with 488 nm, 561 nm, and 635 nm wavelength lasers. Gains for the lasers were set while imaging preablated fish, and UV cone-ablated fish were imaged using the same gains with a pixel dwell of 6 µs.

All analysis and measurements of the histological sections were done on EZ-C1 3.90 Freeviewer (Nikon Corporation, Tokyo, Japan). A total of three fish were examined for each timepoint, with the exception of the 28-day timepoint, which had two fish examined with histology due to poor sectioning. For histological cone counts and ONL thickness, three 200-µm sections were cropped for each fish and the blue and UV cones manually counted from these sections. Sections stained with TO-PRO-3 had three measurements of ONL thickness averaged for each fish. With monocyte histology slides, three 200-µm sections were also identified for each fish, except the pre-ablated, 1 DPA, and 3 DPA fish which each had eight 200-µm sections counted because of poor staining on some slides. Monocytes were classified as "amoeboid" if the cell body was rounded, with fewer than three short processes, whereas "ramified" monocytes had elongated cell bodies with multiple, thin processes.

Statistics

All statistical analysis was performed on Prism 8.0.0 (GraphPad, La Jolla, CA). Normality was evaluated with the Shapiro-Wilk test. UV cone estimates from OCT were analyzed using a Brown-Forsythe and Welch analysis of variance (ANOVA), all monocyte measurements were analyzed using a mixed-effects ANOVA and histologica cone differences were analyzed using a paired *t*-test.

Results

Histological Examination After UV Cone Ablation Shows Variable UV Cone Regeneration and No Change in Blue Cones

Preablated zebrafish showed a repeating pattern of UV and blue cones in a 1:1 ratio, with the pedicles forming a distinct layer in the outer plexiform layer (Fig. 1A). One day after metronidazole-mediated ablation of the UV cones, the mCherry signal is still observed in histological images, but it is greatly reduced compared with preablated fish (Fig. 1B). The blue cones displayed abnormal outer segment morphology with elongated outer segments. However, the blue cones maintained the position of their pedicles, whereas the UV pedicles were retracted. Previous studies have found that pedicle retraction is seen in degenerating cells,[43] suggesting that the UV cones have undergone more permanent damage, whereas the blue cones appeared to be reacting to the changes in adjacent cells in the retina. At 3 DPA, only tiny blebs remained of the UV cones (Fig. 1C), whereas the blue cones still were seen at regular intervals. At 7 DPA, no UV cones (mCherry signal) were observed (Fig. 1D). However, two weeks after ablation (Fig. 1E), UV cones were observed using histology images, but at a greatly reduced density compared to that measured in the non-cone-ablated fish.

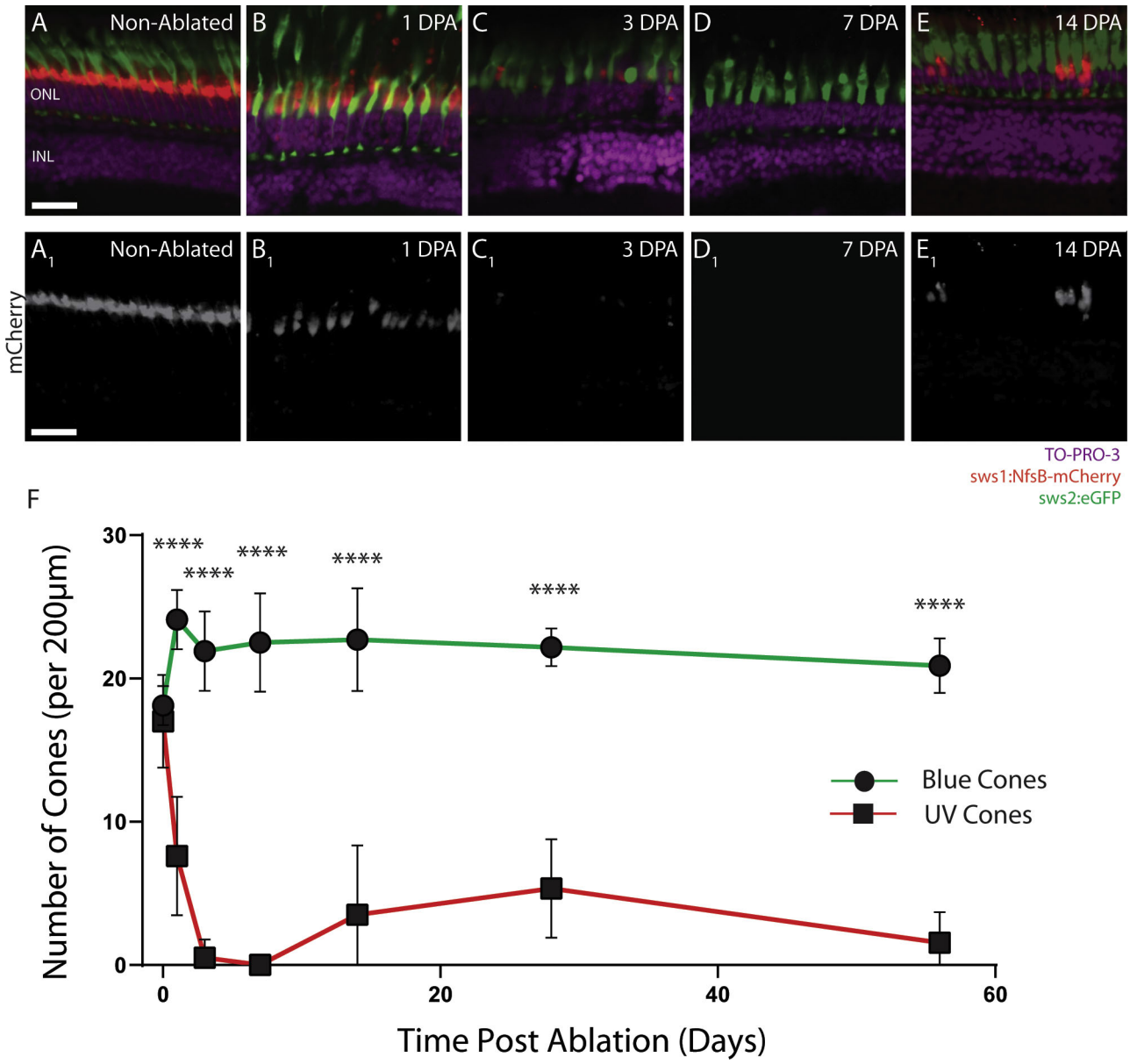

Figure 1. Retinal histology shows loss and regeneration of UV Cones after metronidazole treatment in *sws1:nfsB-mCherry;sws2:eGFP* zebrafish. Non-cone-ablated fish (A) show UV (*sws1*) and blue (*sws2*) cones with regular spacing and morphology. At 1 DPA (B), the outer segments of UV and blue cone show blebbing and elongation, but the pedicles have only retracted in the UV cones. At 3 DPA (C), the blue cones seem to have regained normal outer segment morphology, and only remnants of the UV cones remain. At 7 DPA, no UV cones were observed using histology (D). UV cones are observed to have regenerated by 14 DPA (E), but at a reduced number compared to the preablated UV cone density. By 3 DPA, UV cones have dramatically decreased, and there are significantly fewer UV cones (F). *Scale bar:* 25 µm. ONL, outer nuclear layer; INL, inner nuclear layer. $^{*}P < 0.05$; $^{**}P < 0.01$; $^{***}P < 0.001$; $^{****}P < 0.0001$.

The absolute number of blue cones was unchanged following metronidazole treatment, whereas UV cone numbers decreased to zero and regenerated to diminished levels by 14 DPA (Fig. 1F). As expected, there were no significant differences between the UV and blue cone numbers in non-cone-ablated animals ($P = 0.33$, paired t-test), but significant differences between UV and blue cone numbers were observed at all post-ablation timepoints (DPA1, $P < 0.0001$; DPA3, $P < 0.0001$; DPA7, $P < 0.0001$; DPA14, $P < 0.0001$; DPA28, $P = 0.0001$; DPA56, $P < 0.0001$, paired t-tests).

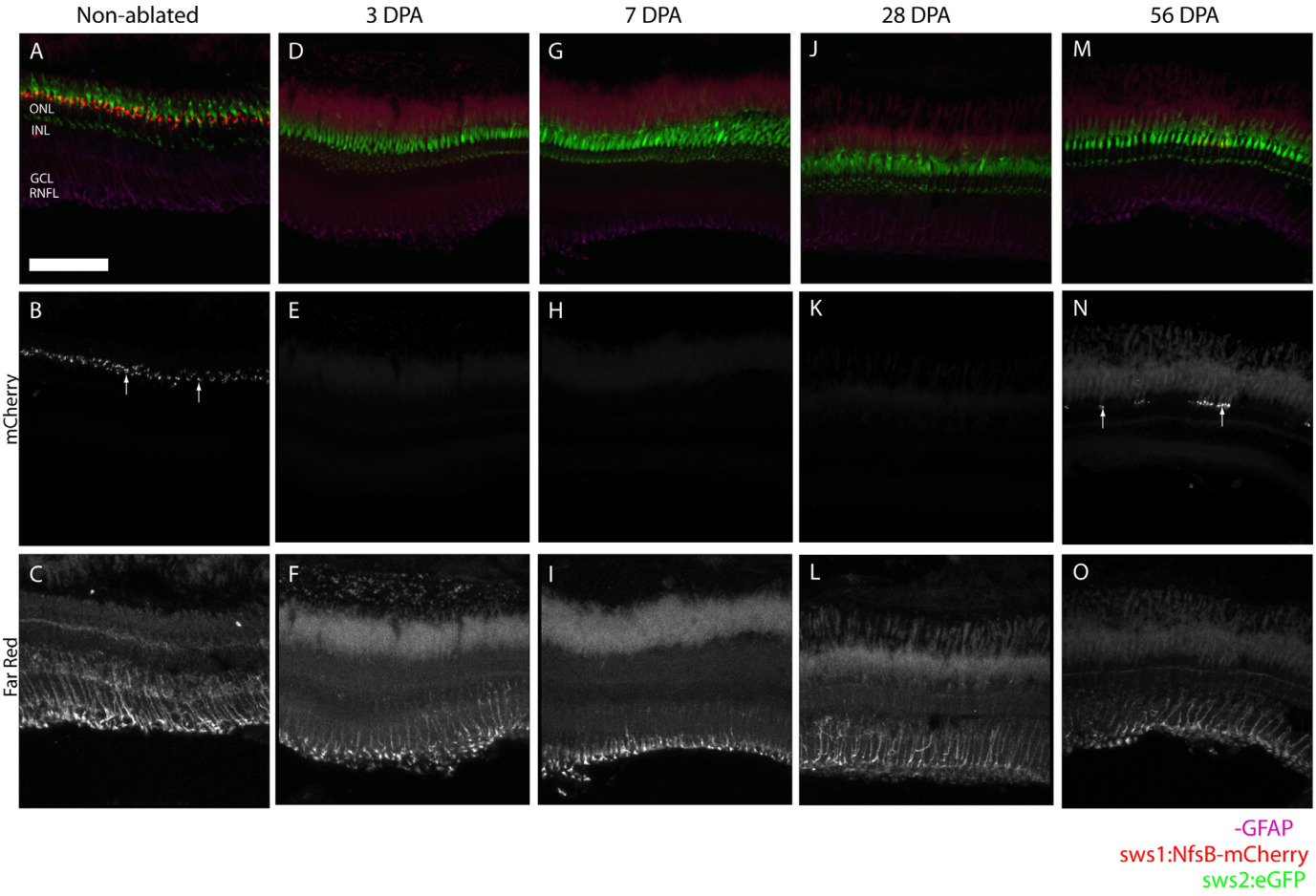

Figure 2. Histology shows no increase in GFAP staining and Müller cell activation after metronidazole treatment. Untreated zebrafish (A) show a continuous UV cone mosaic (B, *arrows*) and baseline Müller cell activation (C). At 3 DPA (D), UV cones aren't observed (E) and no increased in Müller cell activation is seen (F). Similarly, at 7 DPA and 28 DPA (G,J), histology shows no UV cones (H, K) and no Müller cell activation (I, L). At 56 DPA (M), some UV cone regeneration is observed (N, arrows), though the UV cone mosaic is not regular. Despite the UV cone regeneration, no increased in Müller cell activation is observed from GFAP staining (O). *Scale bar*: 100 µm.

Limited Müller Cell Activation Occurs Following Metronidazole Treatment

Previous studies by Fraser et al.[37] show that Müller cells proliferate after widespread retinal damage and subsequent regeneration. However, there is some debate about whether a certain threshold of retinal degeneration or damage is needed for Müller cell activation and subsequent regeneration.[44] We performed GFAP antibody staining to identify Müller cell activation in the post-treatment zebrafish. In nontreated fish (Figs. 2A–C), we observed Müller glia at baseline, with GFAP staining most prominently on the end processes (Fig. 2C). At 3DPA, no UV cones were observed in fluorescent microscopy images (Figs. 2D, 2E) and GFAP staining was still observed in the end processes, not spread throughout the cell body to the photoreceptors (Fig. 2F). Histology of the retina was similar at 3DPA and 7DPA (Figs. 2G–I), and 28DPA (Figs. 2J–L), with GFAP staining primarily at the end processes in all conditions. At 56 DPA (Figs. 2M–O), UV cone regeneration was observed (Fig. 2N) even though GFAP staining restricted to the processes suggests that there has not been substantial Müller cell activation (Fig. 2O).

Variability in UV Cone Regeneration Observed Via OCT

Cone photoreceptors can be visualized postmortem with histology, but OCT offers a method for in vivo cone visualization. Zebrafish OCT images of preablated fish (Figs. 3A–C) showed a regular, cone mosaic which fits the expected crystalline distribution. At 1DPA, the OCT signal was diffuse and no clear

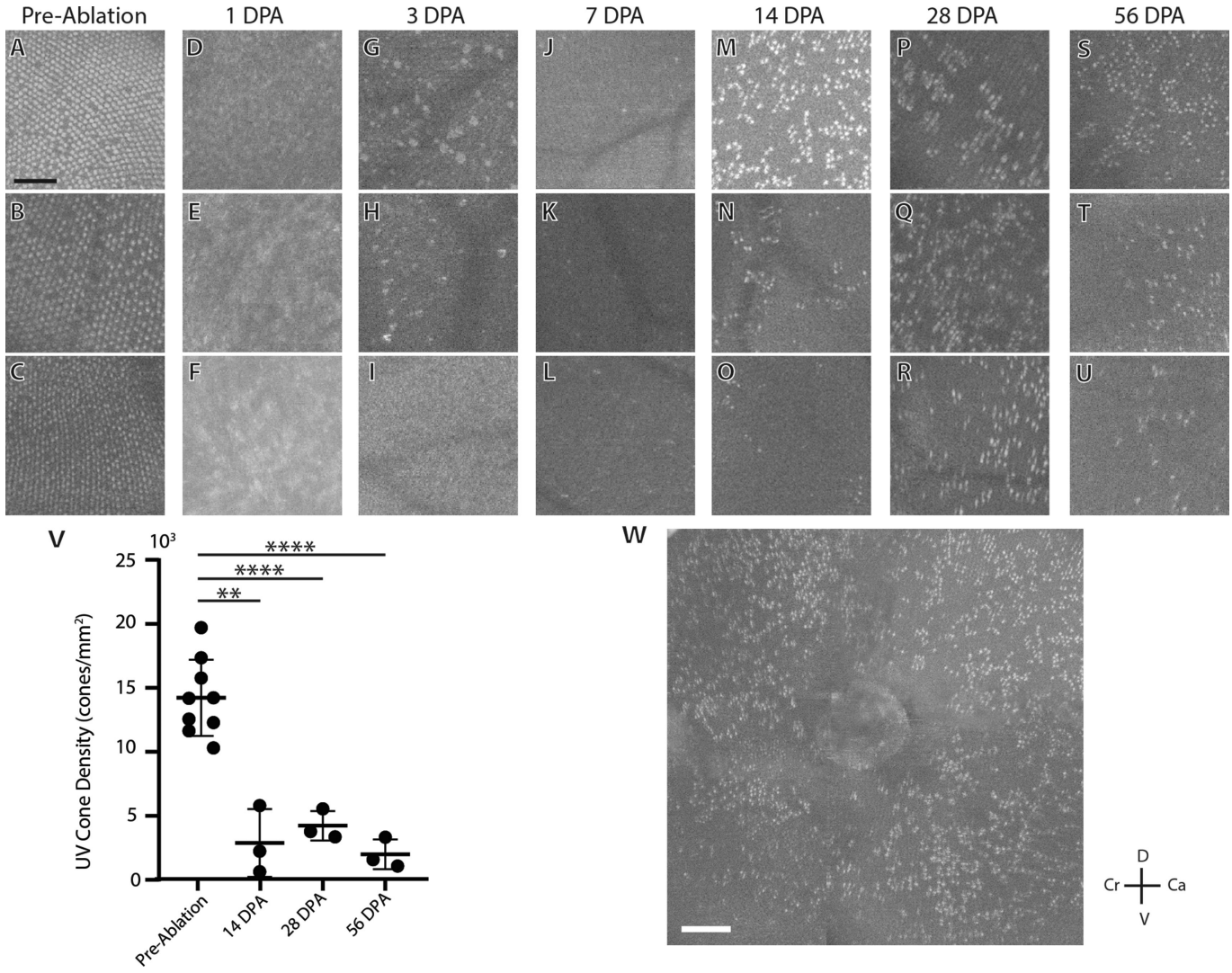

Figure 3. Cross-sectional variability in the UV cone mosaic. Each image shown is a retina from separate fish, except for panel W, which shows a larger montage of panel M. Pre-cone-ablated zebrafish (A, B, C) show a regular UV cone mosaic. At 1 DPA (D–F), no cones are observed in any of the fish. At 3 DPA (G–I), cones are still not observed, but large, hyperreflective inclusions can be observed in some fish (G, H). Individual UV cones are observed at 7 DPA (J–L) and by 14 DPA (M–O) regenerated UV cones show a wide range of cone densities and an irregular clumping pattern. Irregular reflective cones are still observed at 28 DPA (P–R) and 56 DPA (S–U). UV cone density measured from OCT is significantly decreased at 14, 28, and 56 DPA (V). A montage of a fish 14 DPA shows that UV cone regeneration does not follow a gradient and occurs equally across the retina (W). D, dorsal; V, ventral; Cr, cranial; Ca, caudal. *Scale bars*: 50 µm (A–U) and 100 µm (W). $^{*}P < 0.05$; $^{**}P < 0.01$; $^{***}P < 0.001$; $^{****}P < 0.0001$.

structure could be observed (Figs. 3D–F), precluding accurate cone counts. At 3 DPA (Figs. 3G–I), large hyperreflective signals were observed in two fish but were too large to be cones. At 7 DPA (Figs. 3J–L), the hyperreflective signal was not observed, but individual cones were observed. By 14 DPA, cone number had increased, though the cones were clustered with a varied number of cones between fish (Figs. 3M–O). Fish at 28 DPA (Figs. 3P–R) and 56 DPA (Figs. 3S–U) continued to show variable UV cone regeneration with the regenerated UV cones arranged in clusters (Supplementary Fig. S1). UV cone counts from OCT images of the same fish before and after ablation (Fig. 3V) showed significantly decreased UV cone density at 14DPA, 28DPA, and 56 DPA (11.3%, 26.3%, and 10.1% of expected UV cone density; $P = 0.0035$, $P < 0.0001$, $P < 0.0001$, Brown-Forsythe and Welch ANOVA). A larger montage of a single retina at 14 DPA (Fig. 3W) showed clustered cones, with no apparent nasal-temporal or dorsal-ventral gradient.

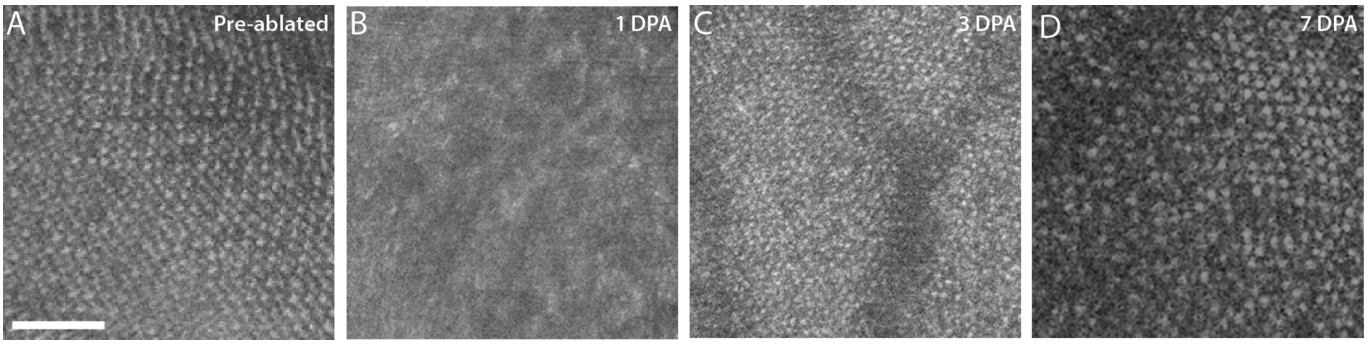

Figure 4. OCT shows changes to the blue cone mosaic after UV cone ablation. The unablated blue cone mosaic (A) shows a regular array of cones, but OCT en face images of the blue cones at 1DPA (B) show diffuse, hyperreflective signal. En face overlays from 3 DPA (C) show blue cones beginning to recover their punctate appearance, and by 7 DPA (D), the blue cone mosaic begins to regain its regular appearance. All images are from separate fish; the UV cone mosaic in panels B,C, and D are shown in Figure 3 as panels E, H, and L, respectively. *Scale bars*: 50 µm.

Changes to the Blue Cone Mosaic After Ablation of the UV Cones

Fish showed distinct changes in the blue cone outer segments after metronidazole-mediated ablation of the UV cones. Although cone numbers did not change (Fig. 1), OCT showed that ablation of the UV cones seemed to transiently affect the blue cone mosaic. In a preablated fish, the blue cone mosaic was highly regular (Fig. 4A), but at just 1 DPA, the blue cone mosaic took on more diffuse character and individual photoreceptors were indistinct (Fig. 4B). This change was transient and at 3 DPA, the blue cone layer regained a more normal appearance when observed with OCT imaging and the cone mosaic appeared more uniformly spaced with normal reflectivity profiles (Fig. 4C). By 7DPA, the blue cone mosaic appeared crystalline with individually distinct photoreceptors and normal reflectivity. The cones at 7 DPA were more easily visualized compared to the pre-cone-ablated fish (Fig. 4D). The diffuse character of the blue cone layer observed in OCT images correlated with the elongated outer segment morphology observed via histology, suggesting that punctate signal seen in OCT images may be related to preserved cone morphology.

Retinal Hyperreflectivites Observed Via OCT

Before ablation, zebrafish OCT showed normal cone morphology (Fig. 5A), and the ONL and IPL layers (Fig. 5B) were homogeneous with no areas of hyperreflectivity (Fig. 5C). OCT images of the same fish at 3 DPA showed focal hyperreflectivities of unknown origin in the INL, ONL and OPL (Fig. 5D). *En face* images generated from the INL, ONL, and OPL (Fig. 5E) showed these hyperreflective inclusions across the retina (Fig. 5F). To investigate whether hyperreflective inclusions could potentially be activated monocytes mounting a response to the UV cone ablation, we performed immunohistochemistry against monocytes using 4C4 antibody.[42]

In preablated zebrafish, histology showed that monocytes usually had ramified morphology and were stratified throughout the inner retinal layers (Fig. 6A). However, starting at 1 DPA, monocytes moved to the outer retinal layers and took on an activated, amoeboid appearance (Fig. 6B); this distribution and morphology were maintained through 3 DPA (Fig. 6C). However, by 7 DPA, the monocytes reverted to a ramified morphology and shifted back to the inner retinal layer (Fig. 6D). The monocytes maintained the ramified morphology and inner retinal distribution at 14, 28, and 56 DPA (Figs. 6E–G). A significant shift from ramified to amoeboid morphology is observed from 1-3 DPA (Figs. 6H–J) along with a significant increase in the number of monocytes in the outer retinal layers (Figs. 6K–M). The time course observed with histology suggested that the nonphotoreceptor hyperreflectivity observed in OCT could potentially be activated monocytes, although further studies are needed to validate this hypothesis.

Discussion

Here we explore OCT imaging as a tool for observing UV cone ablation and subsequent UV cone regeneration in the living zebrafish retina. We also perform correlative histology to aid in the interpretation of our OCT findings. By OCT we observed hyperreflective signal in the retina at one and three days after

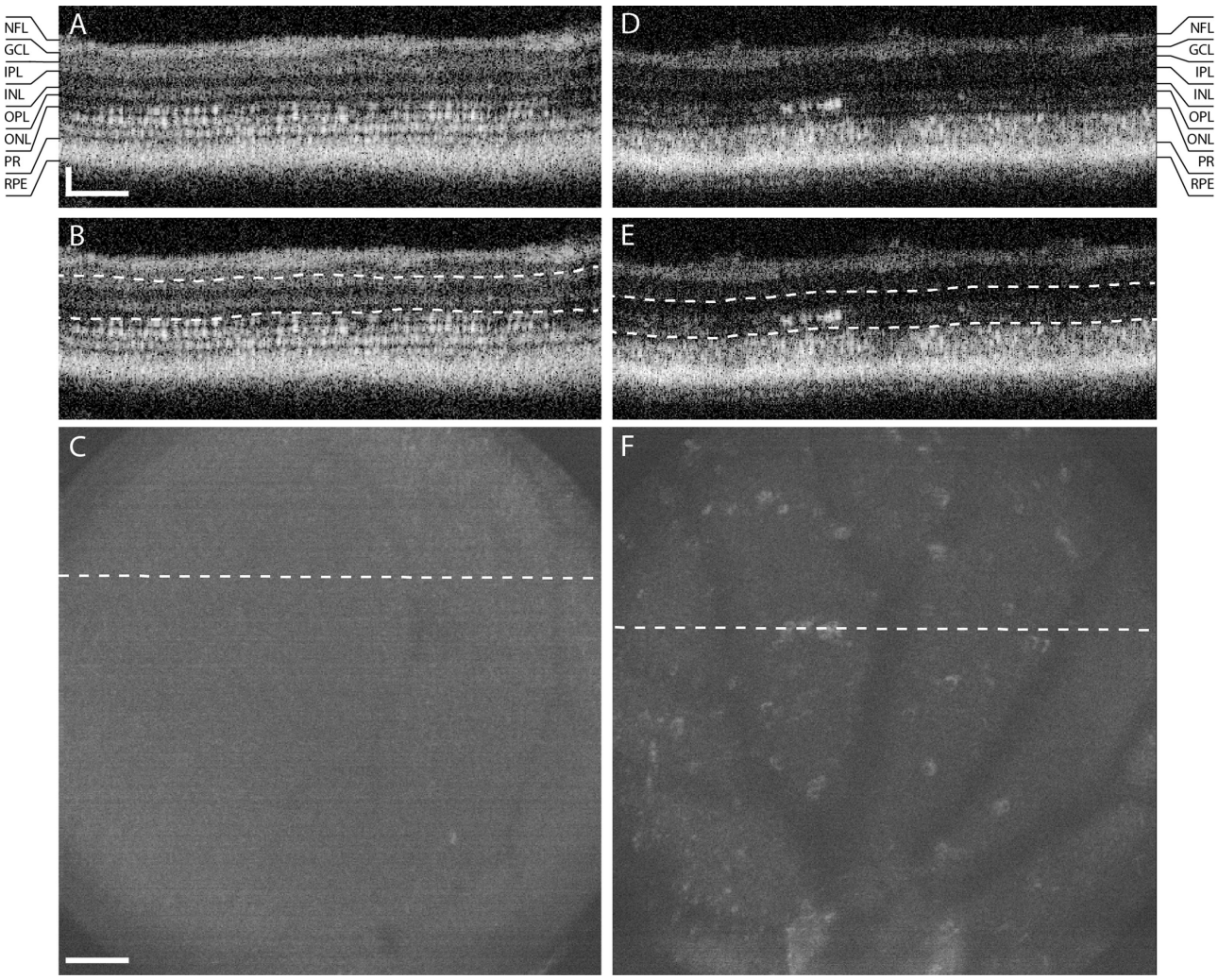

Figure 5. OCT shows inner retinal inclusions in post-ablation zebrafish. An OCT B-scan prior to UV cone ablation (A) shows intact cone structure. The en face image from the ONL to the INL (B, *dashed lines*), shows a homogenous low-intensity image (C, *dashed line* indicates the location of A). In the same fish at 3 DPA, B scans show hyperreflective signal in the ONL (D). The corresponding en face image shows that these inclusions can be seen across the volume (F, location of D indicated by *dashed lines*). *Scale bar*: 50 µm axially and laterally.

metronidazole treatment and correlative histology suggests that this hyperreflective signal may originate from activated monocytes. Additionally, en face images of the blue cone mosaic show a loss of distinct cone signal whereas synchronous correlative histology shows outer segment malformations. These findings suggest that OCT may have the capacity to reveal changes in cone reflectivity and distribution, as well as monocyte recruitment and activation. Collectively, these findings suggest that OCT could be a useful tool for studying the biological basis of cone regeneration in zebrafish.

To our knowledge, several other studies use OCT to evaluate retinal damage in zebrafish.[26,30,45–48] The study by Bailey et al.[26] uses pan-retinal models of damage (retinal ablation with light and ouabain injection) and analyzes retinal changes from B-scans. Weber et al.[30] uses both diffuse light and focused light approaches to ablate the retina. Several groups use a focal laser injury and tracked the lesion with OCT.[45,47,48] Zebrafish retinas ablated with light show a fuzzy appearance of the photoreceptor layers on B-scans at 1 to 4 DPA, similar to what we observed in our images at 3 DPA. The study by Bailey et al.[26] also observes recovery of distinct photoreceptor bands in OCT B-scans at one week after ablation and hyperreflectivity in the ONL after photoreceptor ablation, similar to what we observed. Without virtual en face reconstruction, however, it is difficult to interpret these changes. Additionally, other histological ablation studies have shown monocyte activation results similar to those observed in this study.

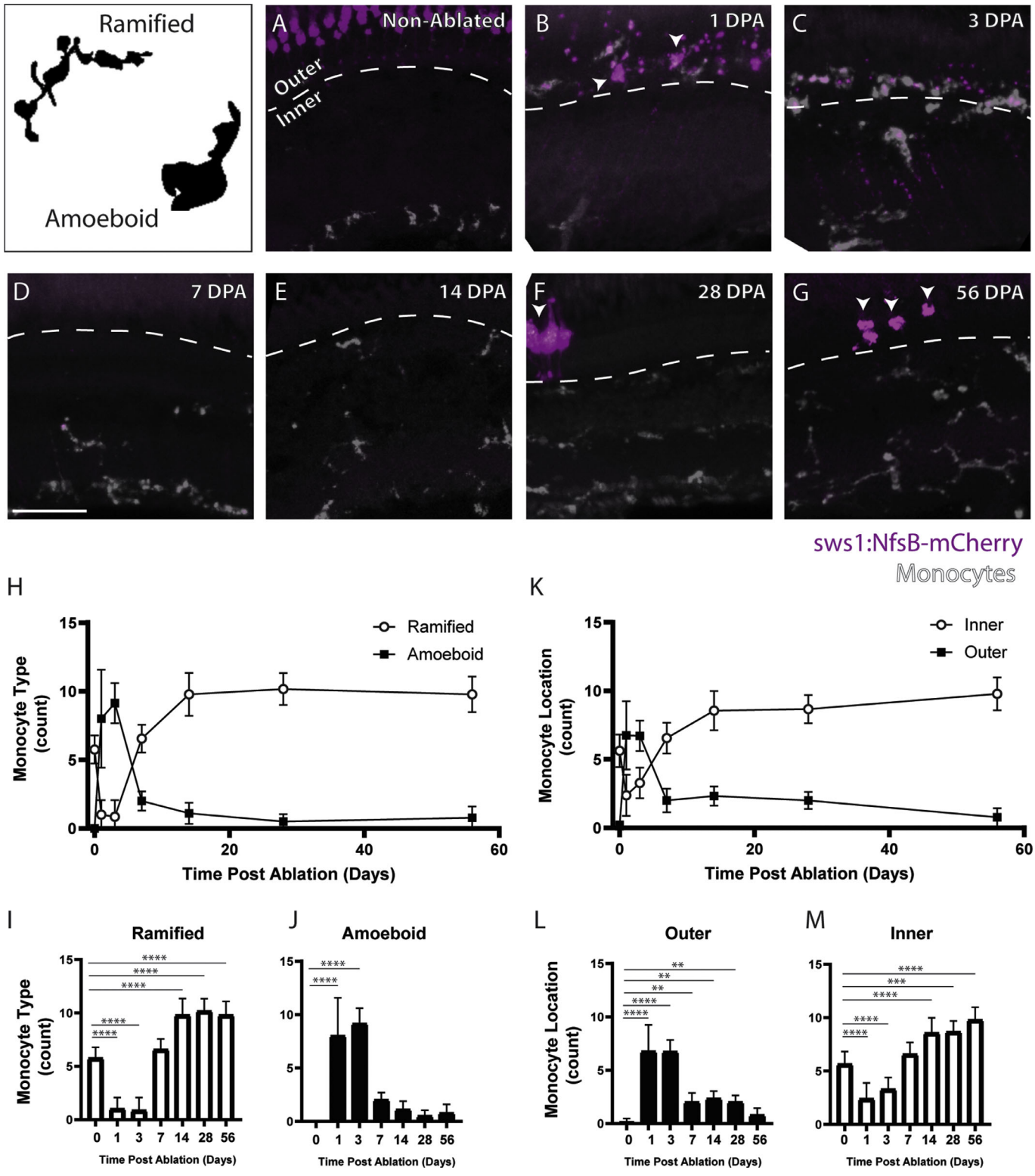

Figure 6. Histology shows a change in monocyte location and morphology after metronidazole-mediated ablation of UV cones. In nonablated retinas (A), monocytes are observed to have a largely ramified morphology and to be distributed largely throughout the inner retinal layers and UV cones appear to have a normal morphology. At 1 DPA, monocytes have largely switched to an amoeboid appearance and translocated to the outer retina (*dashed line*, B); the cones at 1 DPA have begun to form blebs and lack the typical cone morphology (B, *arrows*). Monocytes at 3 DPA continue to have a largely amoeboid appearance and to be in the outer retinal layers (C). The cones at 3 DPA have been largely cleared, and only a few small blebs remain. By 7 DPA, the cones have been completely cleared, and the monocytes have returned to the inner retina with a ramified morphology (D) and remain in this state at 14 DPA (E), 28 DPA (F), and 56 DPA (G). Regenerated →

←
UV cones are observed at 28 and 56 days after ablation (F, G, *arrows*). Graphs of monocyte morphology (H–J) and location (K–M) show the trends observed in histology. Examples of amoeboid and ramified morphology are shown in the *top left panel*. *Scale bar*: 50 µm. $^{*}P < 0.05$; $^{**}P < 0.01$; $^{***}P < 0.001$; $^{****}P < 0.0001$.

Histological ablation studies show a reactive monocyte response after metronidazole-mediated ablation of the central neurons,[49] light ablation of the photoreceptors,[50] and ouabain ablation of the ganglion cell layers.[51] Additionally, monocyte response has been shown to have peaked three days after ouabain ablation,[51] matching the monocyte activation timeline we observe in our study; we similarly also observed a significant increase in monocytes at the degenerating retinal layers. Previous studies demonstrate that macrophages can modulate the regenerative response in fin regeneration.[52] Previous studies by Hagerman et al.[53] using the same zebrafish transgenic line show cone ablation at 1DPA and regeneration at 2DPA. Although this timeline is faster than we observe in our fish, we believe the age difference between the fish (larval fish in Hagerman's study vs. adult fish in our study) can account for these differences. Taken together, these studies suggest that our observations with OCT imaging are repeatable, are not unique to this line of zebrafish, and are a global response that can be seen across multiple zebrafish lines.

However, despite the agreement with previous studies, there are still multiple questions remaining about our monocyte findings. OCT images clearly show the appearance of hyperreflective retinal inclusions that our histology suggests are monocytes. However, neither our histology nor the OCT imaging fully explores the processes occurring in monocytes after metronidazole-mediated cone ablation. Our histology shows that after treatment, there is a shift in monocyte morphology from ramified to amoeboid, indicating monocyte activation. However, we also see an increase in the total number of retinal monocytes, suggesting that monocytes may be recruited to the retina from the choroid or elsewhere. Previous studies show that after ablation of retinal neurons, macrophages are recruited to the retina and proliferate,[51] and it is possible that the monocyte increase observed in our histology is due to a combination of monocyte recruitment and proliferation. Because the 4C4 antibody recognizes macrophages and monocytes of many lineages, it is difficult to define the exact origin of the activated monocytes, although other groups are characterizing and optimizing antibodies that may distinguish the monocyte lineage further.[54,55] However, OCT could be used in tandem with zebrafish inducible-ablation models, such as *mpeg:Gal4 UAS:nfsB-mCherry,* *mpx: Gal4 UAS:nfsB-mCherry,* or *fms (csf1r): Gal4 UAS:nfsB-mCherry* transgenic zebrafish, to explore these questions.[56–58] Petrie et al.[52] have previously published work using a macrophage-specific ablation model which could be used to dissect the retinal immune response following ablation.

Additionally, previous studies by Fraser et al.[37] using the same zebrafish line show that macrophages are actively dividing after UV cone ablation with metronidazole. However, our staining with GFAP does not show Müller cell activation, but it does show regeneration of UV cones. Although other cellular markers such as vimentin were not tested, we do not believe that other markers would reveal any glial cell activation. Further experiments to examine the relationship between UV cone regeneration and Müller cell activation would benefit from a more in vivo approach. Duval et al.[37] use fundus lens imaging with a transgenic fish for cellular-level retinal imaging.[5] Alternatively, one could use either OCT contrast agents, either exogenous or expressed on a transgenic line, for repeated in vivo imaging of cones and Müller glia.[59]

Similarly, our work raises important questions of the etiology of the changes seen in the blue cone mosaic in OCT imaging. After ablation, OCT images show the cone appearance changes to a diffuse, hyperreflective signal that is concomitant with an abnormal cone morphology. This finding suggests that the OCT signal from the cone photoreceptors relies on normal outer segment morphology. Previous studies have explored the waveguiding phenomenon in photoreceptors,[60,61] and other studies done with adaptive optics scanning light ophthalmoscopy have shown that aberrant outer segment structure can impact their reflectivity.[62–64] In a similar manner, the disruption to the blue cone outer segments could disrupt waveguiding enough to alter the appearance of the blue cone en face images.

A limitation of our study is that only the UV cones were assessed in detail, because the more posterior blue and red/green cones are frequently not visible with OCT, possibly because of the limited lateral resolution and signal masking from the more anterior UV cones. The blue cone mosaic was easier to visualize with OCT after UV ablation; however, it is unclear whether blue cone or red/green cone ablation could be tracked with OCT the same way UV cones can. Zebrafish UV cone outer segments are located further

from the RPE than either blue, red, or green cones, whose reflectivity profile may also be confounded by the proximity of the hyperreflective RPE. Additionally, we only imaged our fish at one timepoint after cone ablation, giving a more cross-sectional study design. Although true longitudinal imaging is feasible, because our goal for this study was to optimize our imaging of the zebrafish mosaic, we used high-density OCT scans, in multiple retinal quadrants, under repeated deep anesthesia in quick succession. The combination of these decisions resulted in a relatively high mortality rate per imaging session (~20% in pilot studies, ranging from 0%–75% mortality per imaging session). True longitudinal imaging has been demonstrated in wild-type fish,[28,29] so it should be possible to perform longitudinal imaging of degeneration if OCT scan time is reduced or alternate anesthetic protocols are used. This study examined ablation of a single photoreceptor subtype throughout the retina. Our work leverages several advantages to profiling photoreceptor cell death that will shed light on human retinal disease. First, cones can be ablated at will, and dying, dead, and regenerating photoreceptors can be observed in vivo along with the surrounding cells of the retina. Secondly, targeting of single, isolated cones allows disease processes to be modeled cell by cell, without influence from exogenous disease cues. Lastly, disease processes caused by mutations in cone-specific genes (e.g., achromatopsia, blue cone monochromatism, and X-linked progressive cone dystrophy, or cone-rod dystrophies) can be examined before secondary pathologies affect the rest of the retina. While ablation of a single cone type may be more representative of retinal degenerative diseases, our findings on cone regeneration may not be generalizable to the regeneration in models of panretinal ablation. However, our method for OCT imaging could be used in pan-retinal ablation models. Imaging additional inducible models, such as those targeting colony-stimulating factor receptors, could also be quite valuable in understanding the cellular interactions during both retinal degeneration and regeneration.[65]

In conclusion, we present a method for imaging retinal changes in zebrafish after cone ablation. We demonstrate that OCT is sensitive to monitoring degeneration and regeneration of UV cones. We also observe hyperreflective retinal inclusions, which our correlative histology suggests originates from monocytes, and changing character of the blue cone en face images, which our correlative histology suggests may be caused by morphological changes to the outer segment. Taken together, these findings support OCT as a valuable tool for studying cellular level changes in the zebrafish retina for profiling retinal changes during acute photoreceptor death and for characterizing the regenerative process.

Acknowledgments

The authors thank Pat Cliff, William Hudzinski, and Edi Kuhn for their assistance with zebrafish husbandry. We thank Heather Heitkotter for her assistance with zebrafish degeneration work and Rob Cooper for his assistance with nearest neighbor distance measurements. We express our appreciation to Tatunya Bufford, Christine Duris, and Qiuhui Yang of the Children's Hospital of Wisconsin (CHW) Children's Research Institute (CRI) Histology Core for histology services.

Supported by the National Eye Institute under award numbers F30EY027706, TL1TR001437, P30EY001931, & R01EY016060 and the National Institute of General Medical Sciences of the National Institutes of Health under award number T32GM080202. This investigation was conducted in a facility constructed with support from Research Facilities Improvement Program, Grant Number C06RR016511, from the National Center for Research Resources, National Institutes of Health. The content is solely the responsibility of the authors and does not necessarily represent the official views of the National Institutes of Health. Additional support was provided by the Alcon Research Institute and Foundation Fighting Blindness consortium PPA-0641-0718-UCSF.

Disclosure: **A.L. Huckenpahler,** None; **N.A. Lookfong,** None; **E. Warr,** None; **E. Heffernan,** None; **J. Carroll,** None; **R.F. Collery,** None

References

1. Link BA, Collery RF. Zebrafish models of retinal disease. *Annu Rev Vis Sci*. 2015;1:125–153.
2. Cameron DA. Cellular proliferation and neurogenesis in the injured retina of adult zebrafish. *Vis Neurosci*. 2000;17:789–797.
3. Yurco P, Cameron DA. Responses of Müller glia to retinal injury in adult zebrafish. *Vision Res*. 2005;45:991–1002.
4. Wan J, Goldman D. Retina regeneration in zebrafish. *Curr Opin Genet Dev*. 2016;40:41–47.
5. Duval MG, Chung H, Lehmann OJ, Allison WT. Longitudinal fluorescent observation of retinal

degeneration and regeneration in zebrafish using fundus lens imaging. *Mol Vis*. 2013;19:1082–1095.
6. Campbell LJ, Hyde DR. Opportunities for CRISPR/Cas9 gene editing in retinal regeneration research. *Front Cell Dev Biol*. 2017;5:99.
7. Angueyra JM, Kindt KS. Leveraging zebrafish to study retinal degenerations. *Front Cell Dev Biol*. 2018;6:110.
8. Hamon A, Roger JE, Yang XJ, Perron M. Müller glial cell-dependent regeneration of the neural retina: An overview across vertebrate model systems. *Dev Dynam*. 2016;245:727–738.
9. Lenkowski JR, Raymond PA. Müller glia: stem cells for generation and regeneration of retinal neurons in teleost fish. *Prog Retin Eye Res*. 2014;40:94–123.
10. Adhi M, Duker JS. Optical coherence tomography— current and future applications. *Curr Opin Ophthalmol*. 2013;24:213–221.
11. Jonnal RS, Kocaoglu OP, Zawadzki RJ, Liu Z, Miller DT, Werner JS. A review of adaptive optics optical coherence tomography: technical advances, scientific applications, and the future. *Invest Ophthalmol Vis Sci*. 2016;57:OCT51–OCT68.
12. Kocaoglu OP, Turner TL, Liu Z, Miller DT. Adaptive optics optical coherence tomography at 1 MHz. *Biomed Opt Express*. 2014;5:4186–4200.
13. Liu Z, Kurokawa K, Zhang F, Lee JJ, Miller DT. Imaging and quantifying ganglion cells and other transparent neurons in the living human retina. *Proc Natl Acad Sci USA*. 2017;114:12803–12808.
14. Torti C, Považay B, Hofer B, et al. Adaptive optics optical coherence tomography at 120,000 depth scans/s for non-invasive cellular phenotyping of the living human retina. *Opt Express*. 2009;17:19382–19400.
15. Huber G, Beck SC, Grimm C, et al. Spectral domain optical coherence tomography in mouse models of retinal degeneration. *Invest Ophthalmol Vis Sci*. 2009;50:5888–5895.
16. Fischer MD, Huber G, Beck SC, et al. Noninvasive, in vivo assessment of mouse retinal structure using optical coherence tomography. *PLoS One*. 2009;4:e7507.
17. Abbott CJ, McBrien NA, Gru¨nert U, Pianta MJ. Relationship of the optical coherence tomography signal to underlying retinal histology in the tree shrew (*Tupaia belangeri*). *Invest Ophthalmol Vis Sci*. 2009;50:414–423.
18. Gloesmann M, Hermann B, Schubert C, Sattmann H, Ahnelt PK, Drexler W. Histologic correlation of pig retina radial stratification with ultrahigh-resolution optical coherence tomography. *Invest Ophthalmol Vis Sci*. 2003;44:1696–1703.
19. Sajdak B, Sulai YN, Langlo CS, et al. Noninvasive imaging of the thirteen-lined ground squirrel photoreceptor mosaic. *Vis Neurosci*. 2016;33:e003.
20. Sajdak BS, Salmon AE, Cava JA, et al. Noninvasive imaging of the tree shrew eye: wavefront analysis and retinal imaging with correlative histology. *Exp Eye Res*. 2019;185:107683.
21. Collery RF, Veth KN, Dubis AM, Carroll J, Link BA. Rapid, accurate, and non-invasive measurement of zebrafish axial length and other eye dimensions using SD-OCT allows longitudinal analysis of myopia and emmetropization. *PLoS One*. 2014;9:e110699.
22. Lapierre-Landry M, Huckenpahler AL, Link BA, Collery RF, Carroll J, Skala MC. Imaging melanin distribution in the zebrafish retina using photothermal optical coherence tomography. *Transl Vis Sci Techn*. 2018;7:4.
23. Wilk MA, Huckenpahler AL, Collery RF, Link BA, Carroll J. The effect of retinal melanin on optical coherence tomography images. *Transl Vis Sci Techn*. 2017;6:8.
24. Ustun TE, Iftimia NV, Ferguson RD, Hammer DX. Real-time processing for Fourier domain optical coherence tomography using a field programmable gate array. *Rev Sci Instrum*. 2008;79:114301.
25. Rao KD, Verma Y, Patel HS, Gupta PK. Noninvasive ophthalmic imaging of adult zebrafish eye using optical coherence tomography. *Curr Sci*. 2006;90:1506–1510.
26. Bailey TJ, Davis DH, Vance JE, Hyde DR. Spectral-domain optical coherence tomography as a noninvasive method to assess damaged and regenerating adult zebrafish retinas. *Invest Ophthalmol Vis Sci*. 2012;53:3126–3138.
27. Huckenpahler AL, Wilk MA, Cooper RF, et al. Imaging the adult zebrafish cone mosaic using optical coherence tomography. *Vis Neurosci*. 2016;33:E011.
28. Toms M, Tracey-White D, Muhundhakumar D, Sprogyte L, Dubis AM, Moosajee M. Spectral domain optical coherence tomography: an in vivo imaging protocol for assessing retinal morphology in adult zebrafish. *Zebrafish*. 2017;14:118–125.
29. Huckenpahler A, Wilk M, Link B, Carroll J, Collery R. Repeatability and reproducibility of in vivo cone density measurements in the adult zebrafish retina. *Adv Exp Med Biol*. 2018;1074:151–156.
30. Weber A, Hochmann S, Cimalla P, et al. Characterization of light lesion paradigms and optical coherence tomography as tools to study

adult retina regeneration in zebrafish. *PLoS One*. 2013;8:e80483.
31. Raymond PA, Barthel LK, Bernardos RL, Perkowski JJ. Molecular characterization of retinal stem cells and their niches in adult zebrafish. *BMC Dev Biol*. 2006;6:36.
32. Vihtelic TS, Hyde DR. Light-induced rod and cone cell death and regeneration in the adult albino zebrafish (Danio rerio) retina. *J Neurobiol*. 2000;44:289–307.
33. Liu Q, Londraville RL, Azodi E, et al. Up-regulation of cadherin-2 and cadherin-4 in regenerating visual structures of adult zebrafish. *Exp Neurol*. 2002;177:396–406.
34. Fimbel SM, Montgomery JE, Burket CT, Hyde DR. Regeneration of inner retinal neurons after intravitreal injection of ouabain in zebrafish. *J Neurosci*. 2007;27:1712–1724.
35. Ariga J, Walker SL, Mumm JS. Multicolor time-lapse imaging of transgenic zebrafish: Visualizing retinal stem cells activated by targeted neuronal cell ablation. *JoVE*. 2010;43:2093.
36. D'Orazi FD, Zhao XF, Wong RO, Yoshimatsu T. Mismatch of synaptic patterns between neurons produced in regeneration and during development of the vertebrate retina. *Curr Biol*. 2016;26:2268–2279.
37. Fraser B, Duval MG, Wang H, Allison WT. Regeneration of cone photoreceptors when cell ablation is primarily restricted to a particular cone subtype. *PLoS One*. 2013;8:e55410.
38. Yoshimatsu T, D'Orazi FD, Gamlin CR, et al. Presynaptic partner selection during retinal circuit reassembly varies with timing of neuronal regeneration in vivo. *Nature Commun*. 2016;7:10590.
39. Pisharath H, Rhee JM, Swanson MA, Leach SD, Parsons MJ. Targeted ablation of beta cells in the embryonic zebrafish pancreas using E.coli nitroreductase. *Mech Dev*. 2007;124:218–229.
40. Tanna H, Dubis AM, Ayub N, et al. Retinal imaging using commercial broadband optical coherence tomography. *Br J Ophthalmol*. 2010;94:372–376.
41. Cooper RF, Wilk MA, Tarima S, Carroll J. Evaluating descriptive metrics of the human cone mosaic. *Invest Ophthalmol Vis Sci*. 2016;57:2992–3001.
42. Becker T, Becker CG. Regenerating descending axons preferentially reroute to the gray matter in the presence of a general macrophage/microglial reaction caudal to a spinal transection in adult zebrafish. *J Comp Neurol*. 2001;433:131–147.
43. Lin B, Masland RH, Strettoi E. Remodeling of cone photoreceptor cells after rod degeneration in Rd mice. *Exp Eye Res*. 2009;88:589–599.
44. Lessieur EM, Song P, Nivar GC, et al. Ciliary genes arl13b, ahi1 and cc2d2a differentially modify expression of visual acuity phenotypes but do not enhance retinal degeneration due to mutation of cep290 in zebrafish. *PLoS One*. 2019;14:e0213960.
45. DiCicco RM, Bell BA, Kaul C, et al. Retinal regeneration following OCT-guided laser injury in zebrafish. *Invest Ophthalmol Vis Sci*. 2014;55:6281–6288.
46. Lin Y, Xiang X, Chen T, et al. In vivo monitoring the dynamic process of acute retinal hemorrhage and repair in zebrafish with spectral-domain optical coherence tomography. *J Biophotonics*. 2019;12:e201900235.
47. Conedera FM, Quintela Pousa AM, Mercader N, Tschopp M, Enzmann V. Retinal microglia signaling affects Müller cell behavior in the zebrafish following laser injury induction. *Glia*. 2019;67:1150–1166.
48. Conedera FM, Arendt P, Trepp C, Tschopp M, Enzmann V. Müller glia cell activation in a laser-induced retinal degeneration and regeneration model in zebrafish. *JoVE*. 2017;128:56249.
49. van Ham TJ, Brady CA, Kalicharan RD, et al. Intravital correlated microscopy reveals differential macrophage and microglial dynamics during resolution of neuroinflammation. *Dis Model Mech*. 2014;7:857–869.
50. White DT, Sengupta S, Saxena MT, et al. Immunomodulation-accelerated neuronal regeneration following selective rod photoreceptor cell ablation in the zebrafish retina. *Proc Natl Acad Sci USA*. 2017;114:E3719–E3728.
51. Mitchell DM, Lovel AG, Stenkamp DL. Dynamic changes in microglial and macrophage characteristics during degeneration and regeneration of the zebrafish retina. *J Neuroinflammation*. 2018;15:163.
52. Petrie TA, Strand NS, Tsung-Yang C, Rabinowitz JS, Moon RT. Macrophages modulate adult zebrafish tail fin regeneration. *Development*. 2014;141:2581–2591.
53. Hagerman GF, Noel NCL, Cao SY, Duval MG, Oel AP, Allison WT. Rapid recovery of visual function associated with blue cone ablation in zebrafish. *PLoS One*. 2016;11:e0166932.
54. Martins RR, Ellis PS, MacDonald RB, Richardson RJ, Henriques CM. Resident immunity in tissue repair and maintenance: The zebrafish model coming of age. *Front Cell Dev Biol*. 2019;7:12.
55. Zou S, Tian C, Ge S, Hu B. Neurogenesis of retinal ganglion cells is not essential to visual functional recovery after optic nerve injury in adult zebrafish. *PLoS One*. 2013;8:e57280.

56. Theodore LN, Hagedorn EJ, Cortes M, et al. Distinct roles for matrix metalloproteinases 2 and 9 in embryonic hematopoietic stem cell emergence, migration, and niche colonization. *Stem Cell Rep*. 2017;8:1226–1241.
57. Lai SL, Marín-Juez R, Moura PL, et al. Reciprocal analyses in zebrafish and medaka reveal that harnessing the immune response promotes cardiac regeneration. *eLife*. 2017;20:e25605.
58. Gray C, Loynes CA, Whyte MK, Crossman DC, Renshaw SA, Chico TJ. Simultaneous intravital imaging of macrophage and neutrophil behaviour during inflammation using a novel transgenic zebrafish. *Thromb Haemost*. 2011;105:811–819.
59. Lu GJ, Chou L, Malounda D, et al. Biomolecular contrast agents for optical coherence tomography. *ACS Nano*. 2020;14:7823–7831.
60. Enoch JM. Optical properties of the retinal receptors. *J Opt Soc Am*. 1963;53:71–85.
61. Horowitz BR. Theoretical considerations of the retinal receptor as a waveguide. In: Enoch JM, Tobey FL, Jr (eds), *Vertebrate Photoreceptor Optics*. Berlin: Springer-Verlag; 1981:219–300.
62. Langlo CS, Patterson EJ, Higgins BP, et al. Residual foveal cone structure in *CNGB3*-associated achromatopsia. *Invest Ophthalmol Vis Sci*. 2016;57:3984–3995.
63. Scoles D, Sulai YN, Cooper RF, et al. Photoreceptor inner segment morphology in Best vitelliform macular dystrophy. *Retina*. 2016;37:741–748.
64. Carroll J, Dubra A, Gardner JC, et al. The effect of cone opsin mutations on retinal structure and the integrity of the photoreceptor mosaic. *Invest Ophthalmol Vis Sci*. 2012;53:8006–8015.
65. Eom DS, Parichy DM. A macrophage relay for long-distance signaling during postembryonic tissue remodeling. *Science*. 2017;355:1317–1320.